Supporting Information

Zeolitic-imidazolate frameworks derived Ni-Co layered double hydroxide hollow microspheres with enhanced pseudocapacitive properties for hybrid supercapacitors

Xu Li [a, b], Shuangyi Liu [b], Sihan Bai [b], Zhenhu Li *[b], Jun Shen *[a]

[a]*State Key Laboratory of Mechanical Transmission, College of Materials Science and Engineering, Chongqing University, Chongqing, 400044, P.R. China*

[b]*Chongqing Key Laboratory of Multi-Scale Manufacturing Technology, Chongqing Institute of Green and Intelligent Technology, Chinese Academy of Sciences, Chongqing 400714, P.R. China*

Email: shenjun@cqu.edu.cn; lizhenhu@cigit.ac.cn

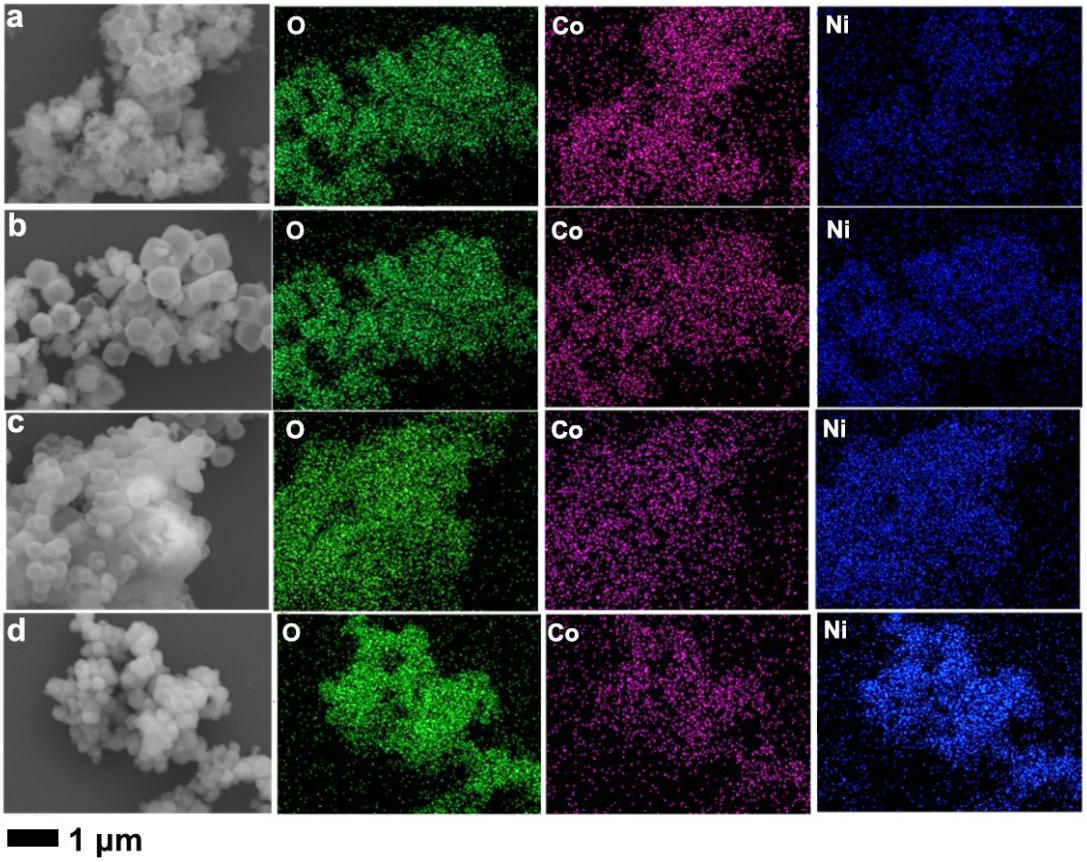

Figure S1 EDS elemental mapping images of O, Co and Ni of (a) Ni-Co-LDH-C-1:4, (b) Ni-Co-LDH-C-1:1, (c) Ni-Co-LDH-C-2:1 and (d) Ni-Co-LDH-C-4:1.

Table S1 The ratio of Ni and Co atomic ratio of Ni-Co-LDH-C-1:4, Ni-Co-LDH-C-1:1, Ni-Co-LDH-C-2:1 and Ni-Co-LDH-C-4:1 determined by ICP-OES.

Sample	Ni (Atomic %)	Co (Atomic %)	Ni / Co atomic ratio
Ni-Co-LDH-C-1:4	22.8	77.2	1:3.4
Ni-Co-LDH-C-1:1	57.8	42.2	1.4:1
Ni-Co-LDH-C-2:1	67.7	32.3	2.1:1
Ni-Co-LDH-C-4:1	81.8	18.2	4.5:1

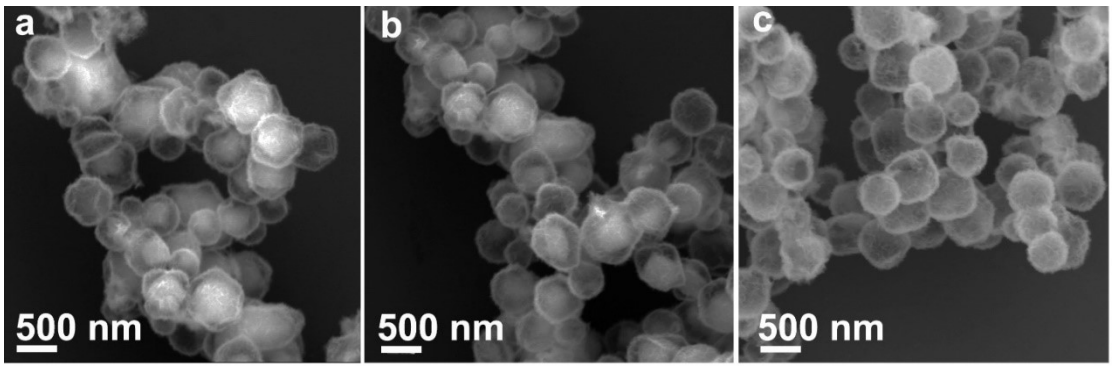

Figure S2 Time-dependent SEM images of the products collected at different reaction stages: Ni-Co-LDH-C-4:1 for 20 min (a), 40 min (b) and 2 h (c).

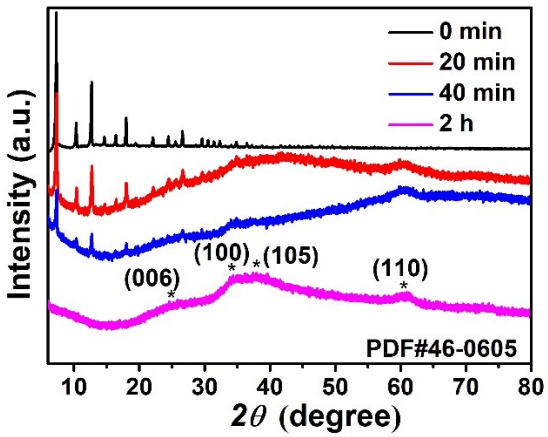

Figure S3 XRD patterns of Ni-Co-LDH-C-4:1 collected at different reaction stages.

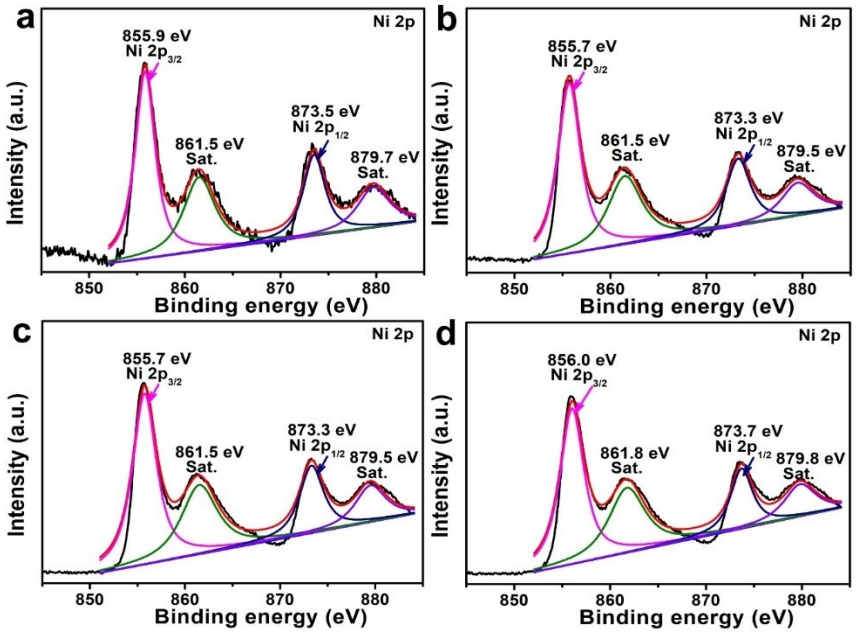

Figure S4 The high resolution XPS spectra for Ni 2p of (a) Ni-Co-LDH-C-1:4, (b) Ni-Co-LDH-C-1:1, (c) Ni-Co-LDH-C-2:1 and (d) Ni-Co-LDH-C-4:1.

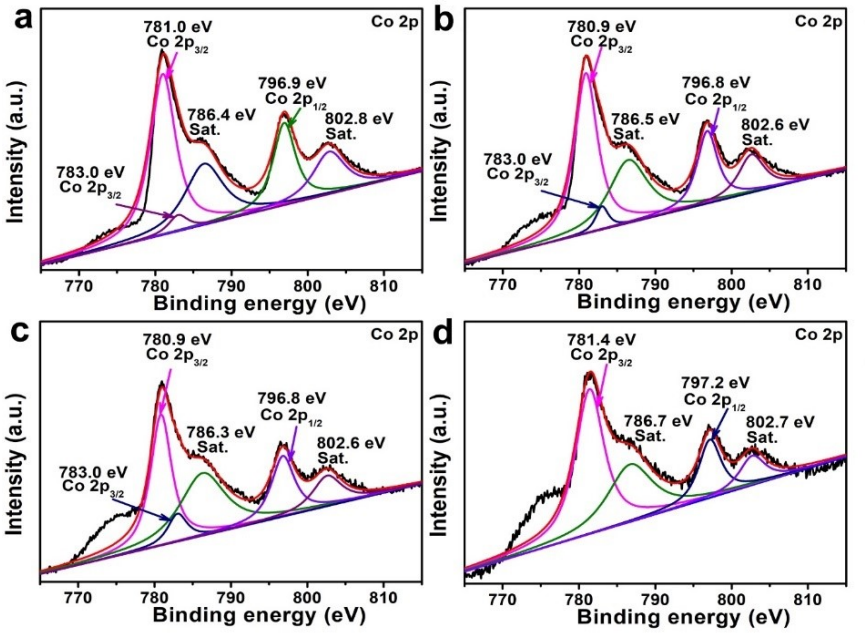

Figure S5 The high resolution XPS spectra for Co 2p of (a) Ni-Co-LDH-C-1:4, (b) Ni-Co-LDH-C-1:1, (c) Ni-Co-LDH-C-2:1 and (d) Ni-Co-LDH-C-4:1.

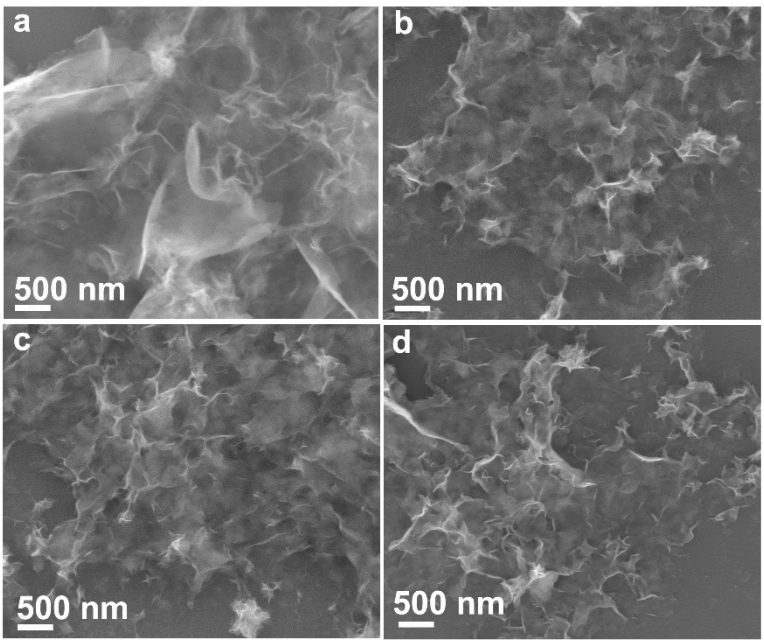

Figure S6 Morphology characterizations of (a) Ni-Co-LDH-W-1:4, (b) Ni-Co-LDH-W-1:1, (c) Ni-Co-LDH-W-2:1 and (d) Ni-Co-LDH-W-4:1.

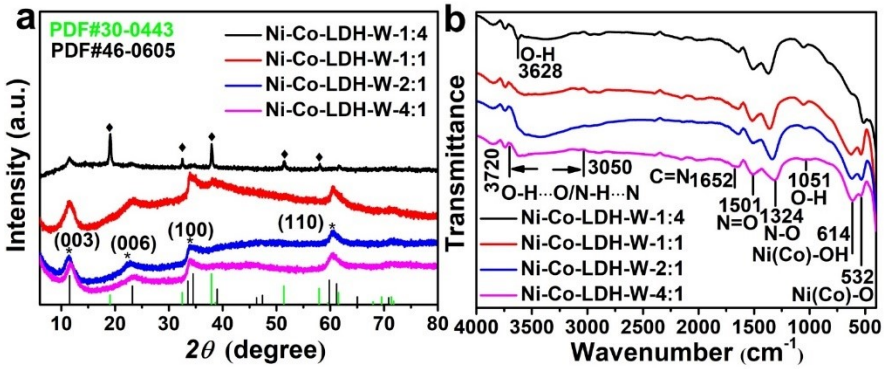

Figure S7 Characterizations of Ni-Co-LDH-W-1:4, Ni-Co-LDH-W-1:1, Ni-Co-LDH-W-2:1 and Ni-Co-LDH-W-4:1. (a) XRD patterns. (b) FT-IR spectra at the wavenumber of 4000-400 cm^{-1}.

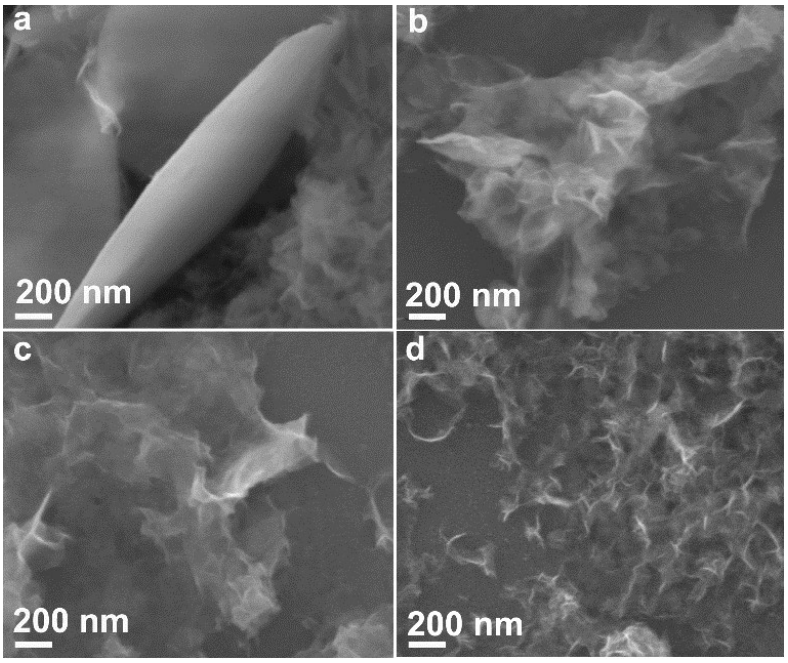

Figure S8 Morphology characterizations of (a) Ni-Co-LDH-L-1:4, (b) Ni-Co-LDH-L-1:1, (c) Ni-Co-LDH-L-2:1 and (d) Ni-Co-LDH-L-4:1.

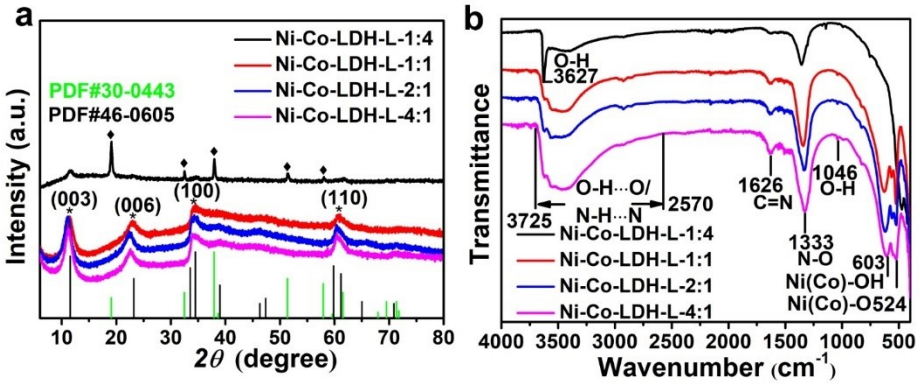

Figure S9 Characterizations of Ni-Co-LDH-L-1:4, Ni-Co-LDH-L-1:1, Ni-Co-LDH-L-2:1 and Ni-Co-LDH-L-4:1. (a) XRD patterns. (b) FT-IR spectra at the wavenumber of 4000-400 cm^{-1}.

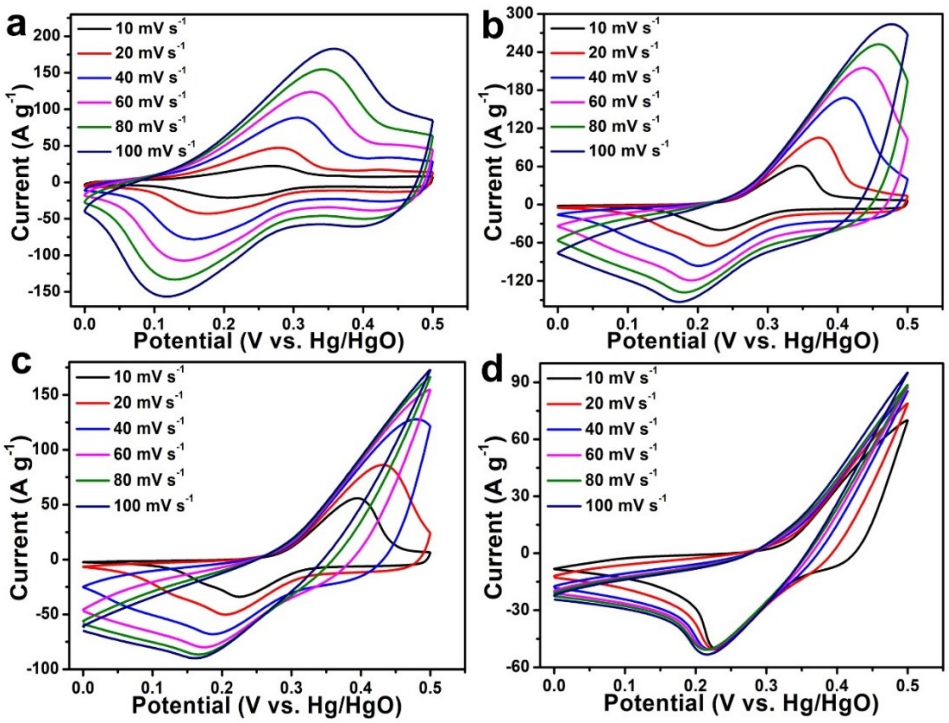

Figure S10 CV curves at different scan rates of (a) Ni-Co-LDH-C-1:4, (b) Ni-Co-LDH-C-1:1, (c) Ni-Co-LDH-C-2:1 and (d) Ni-Co-LDH-C-4:1 electrodes.

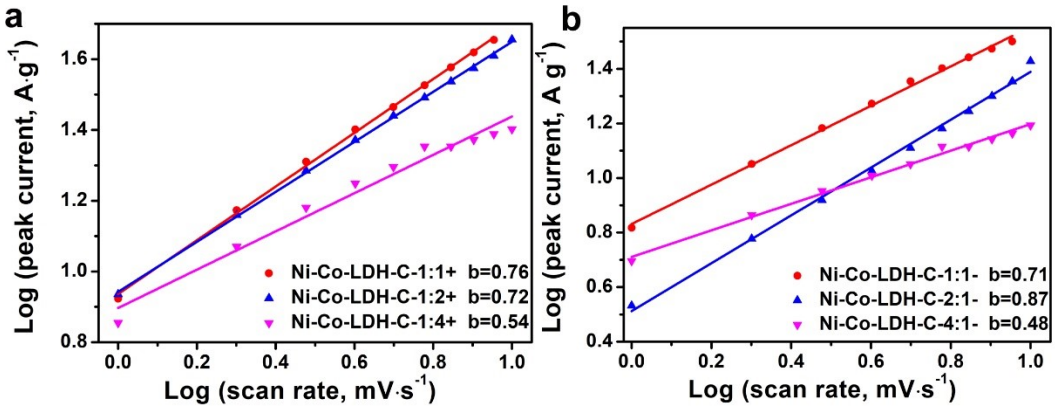

Figure S11 Normalized peak-current plot to determine the b value for anodic (a) and cathodic (b) process of Ni-Co-LDH-C-1:1, Ni-Co-LDH-C-2:1 and Ni-Co-LDH-C-4:1 electrodes.

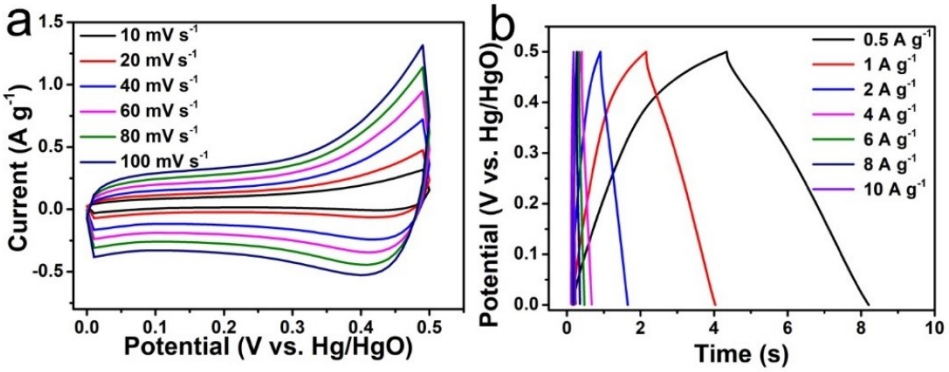

Figure S12 Electrochemical performances of Ni-Co-LDH-C-1:4 electrode. (a) CV curves at different scan rates and (b) GCD curves at different current densities.

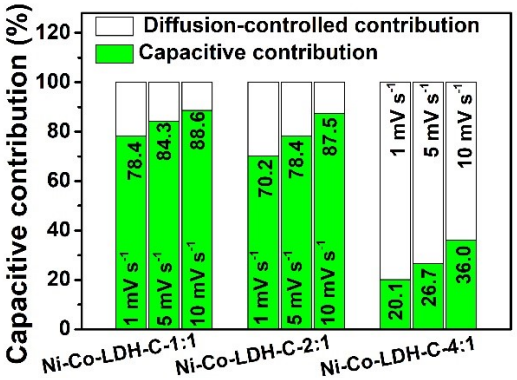

Figure S13 Normalized capacitive and diffusion-controlled contributions to charge storage at different scan rates of Ni-Co-LDH-C-1:1, Ni-Co-LDH-C-2:1 and Ni-Co-LDH-C-4:1 electrodes.

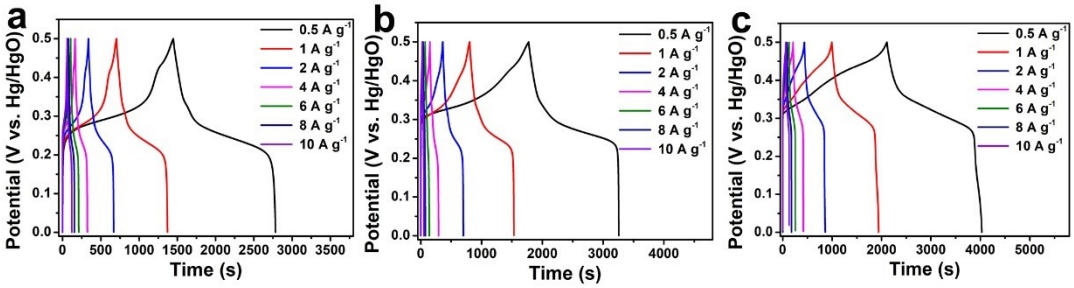

Figure S14 GCD curves at different current densities of (a) Ni-Co-LDH-C-1:1, (b) Ni-Co-LDH-C-2:1 and (c) Ni-Co-LDH-C-4:1 electrodes.

Table S2. Specific capacity at different current densities of Ni-Co-LDH-C-1:4, Ni-Co-LDH-C-1:1, Ni-Co-LDH-C-2:1 and Ni-Co-LDH-C-4:1 electrodes.

Current density (A g^{-1})	Ni-Co-LDH-C-1:4 (mAh g^{-1})	Ni-Co-LDH-C-1:1 (mAh g^{-1})	Ni-Co-LDH-C-2:1 (mAh g^{-1})	Ni-Co-LDH-C-4:1(mAh g^{-1})
0.5	137	193	206	263
1	135	185	202	255
2	134	183	189	243
4	132	178	177	223
6	127	174	171	202
8	126	170	162	182
10	124	166	157	164

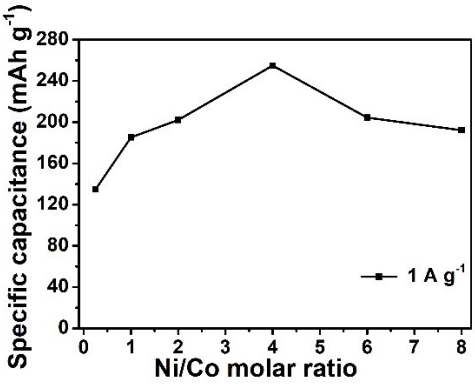

Figure S15 Rate capability varying curve with an increase in the Ni contents of Ni-Co-LDH-C-1:4, Ni-Co-LDH-C-1:1, Ni-Co-LDH-C-2:1, Ni-Co-LDH-C-4:1, Ni-Co-LDH-C-8:1 and Ni-Co-LDH-C-16:1 electrodes at 1A g^{-1}.

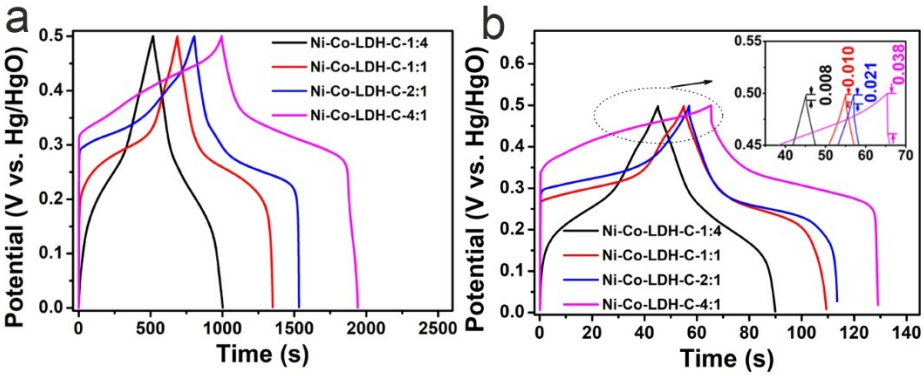

Figure S16 GCD curves of Ni-Co-LDH-C-1:4, Ni-Co-LDH-C-1:1, Ni-Co-LDH-C-2:1 and Ni-Co-LDH-C-4:1 electrodes at 1 A g^{-1} (a) and 10 A g^{-1} (b).

Table S3. Compared performance between Ni-Co-LDH-Cs and other reported materials of high stability.

Materials	**Cycle life**	**Specific capacity/ capacitance**	**Reference**
MnO_2/NGCF	10 000 cycles (100%)	489.7 F g^{-1} (1 A g^{-1})	[1]
$MnSe_2$/rGO	10 000 cycles (99.4%)	326 F g^{-1} (1.5 A g^{-1})	[2]
CoP/P	10 000 cycles (99%)	422.4 C g^{-1} (1 A g^{-1})	[3]
$NiCo_2S_4$ NFs@$NiCo_2S_4$	4000 cycles (92%)	338.1 mAh g^{-1} (1 A g^{-1})	[4]
CeO_2/NiV-LDH (2:2)//Bi_2O_3	10 000 cycles (86.4%)	176 F g^{-1} (2 A g^{-1})	[5]
CoNi-LDH-350P@CFC//active carbon	3000 cycles (87.7%)	223 mAh g^{-1} (0.5 A g^{-1})	[6]
NiCo LDH/$Co(OH)_2$	1000 cycles (92%)	2220.0 F g^{-1} (1 A g^{-1})	[7]
CNTs@NiCo-LDH//ZIF-8	5200 cycles (90.22%)	176.33 mAh g^{-1} (1 A g^{-1})	[8]
CCCH@NiCo-LDH NWAs@Au-CuO/Cu	30 000 cycles (90.8%)	1237 F g^{-1} (1 A g^{-1})	[9]
NiCo-LDH/D-HNTs	2000 cycles (80.8%)	1401.4 C g^{-1} (1 A g^{-1})	[10]
Ni-Co-LDH-C-1:4	10 000 cycles (102%)	135 mAh g^{-1} (972 F g^{-1}, 1 A g^{-1})	**This work**
Ni-Co-LDH-C-1:1	10 000 cycles (89%)	185 mAh g^{-1} (1332 F g^{-1}, 1 A g^{-1})	
Ni-Co-LDH-C-2:1	10 000 cycles (79%)	202 mAh g^{-1} (1454 F g^{-1}, 1 A g^{-1})	
Ni-Co-LDH-C-4:1	10 000 cycles (59%)	255 mAh g^{-1} (1836 F g^{-1}, 1 A g^{-1})	

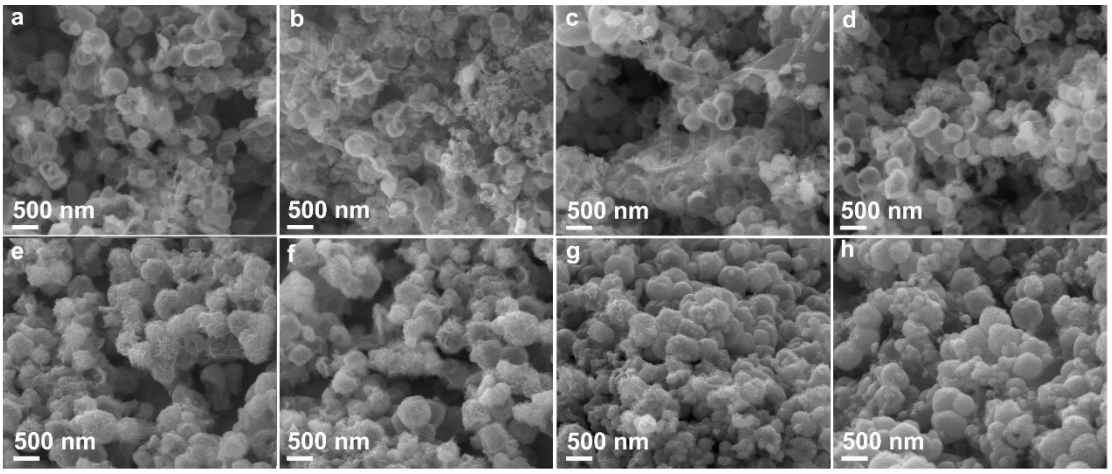

Figure S17 SEM images of Ni-Co-LDH-C-1:4, Ni-Co-LDH-C-1:1, Ni-Co-LDH-C-2:1 and Ni-Co-LDH-C-4:1 electrodes (a, b, c and d) and after the cycling test at 6 A g^{-1}(e, f, g and h).

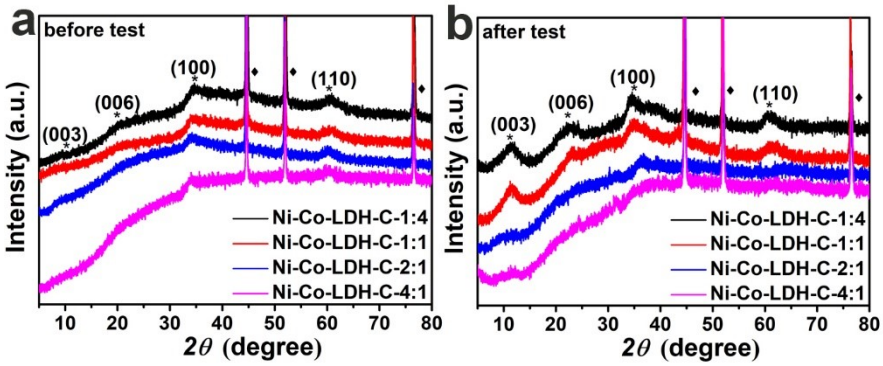

Figure S18 The XRD patterns of Ni-Co-LDH-C-1:4, Ni-Co-LDH-C-1:1, Ni-Co-LDH-C-2:1 and Ni-Co-LDH-C-4:1 electrodes (a) before and (b) after the cycling test at 6 A g^{-1}. Note that the peaks marked with * and ♦ originate from Ni-Co-LDH-Cs and nickel foam, respectively.

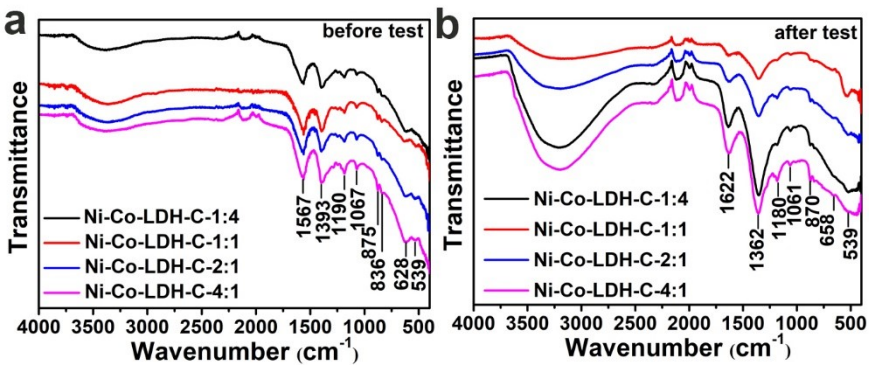

Figure S19 The FT-IR patterns of Ni-Co-LDH-C-1:4, Ni-Co-LDH-C-1:1, Ni-Co-LDH-C-2:1 and Ni-Co-LDH-C-4:1 electrodes (a) before and (b) after the cycling test at 6 A g^{-1}.

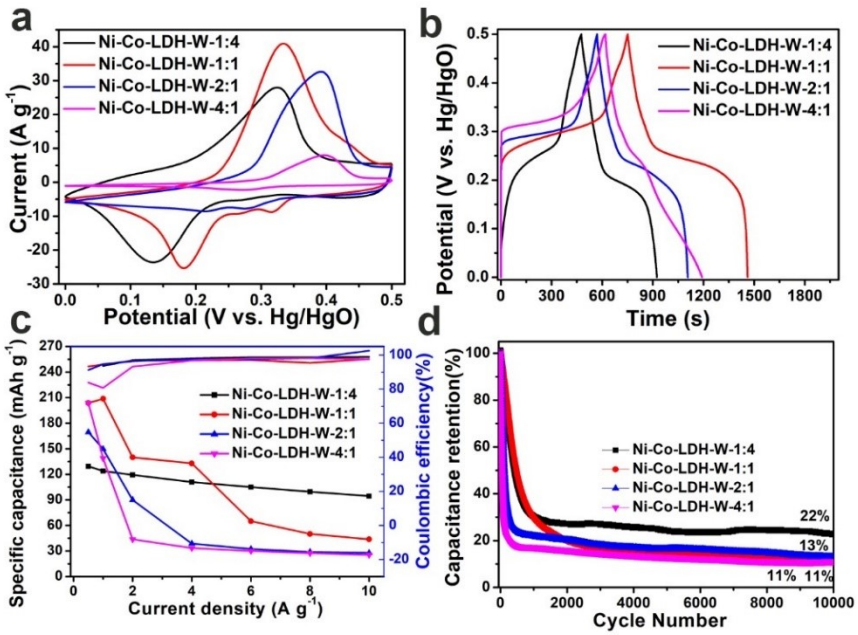

Figure S20 Electrochemical performances of Ni-Co-LDH-W-1:4, Ni-Co-LDH-W-1:1, Ni-Co-LDH-W-2:1 and Ni-Co-LDH-W-4:1 electrodes. (a) CV curves. (b) Galvanostatic charge/discharge curves at the current density of 1 A g^{-1}. (c) Rate capability and coulombic efficiency of the electrodes at current densities from 0.5 to 10 A g^{-1}. (d) Cycling performance at 6 A g^{-1}.

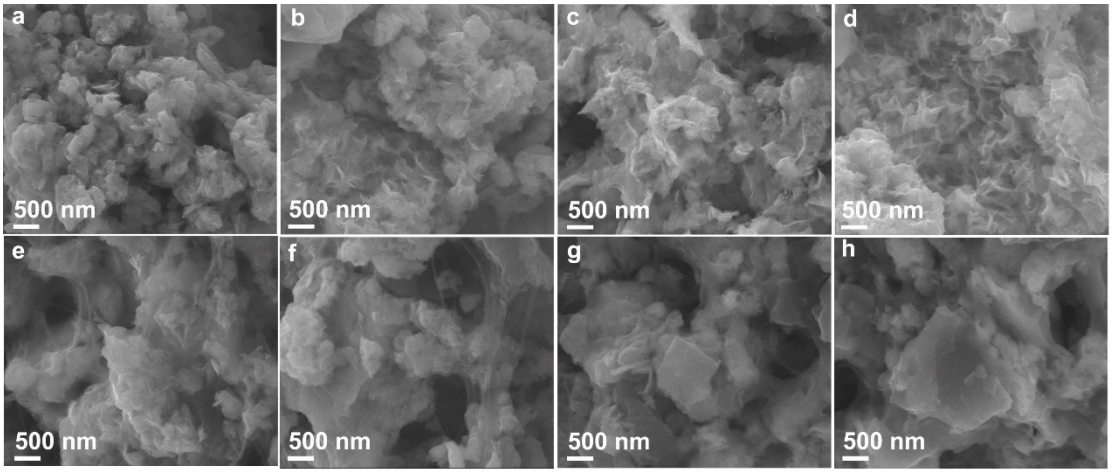

Figure S21 SEM images of Ni-Co-LDH-W-1:4, Ni-Co-LDH-W-1:1, Ni-Co-LDH-W-2:1 and Ni-Co-LDH-W-4:1 electrodes (a, b, c and d) and after the cycling test at 6 A g^{-1}(e, f, g and h).

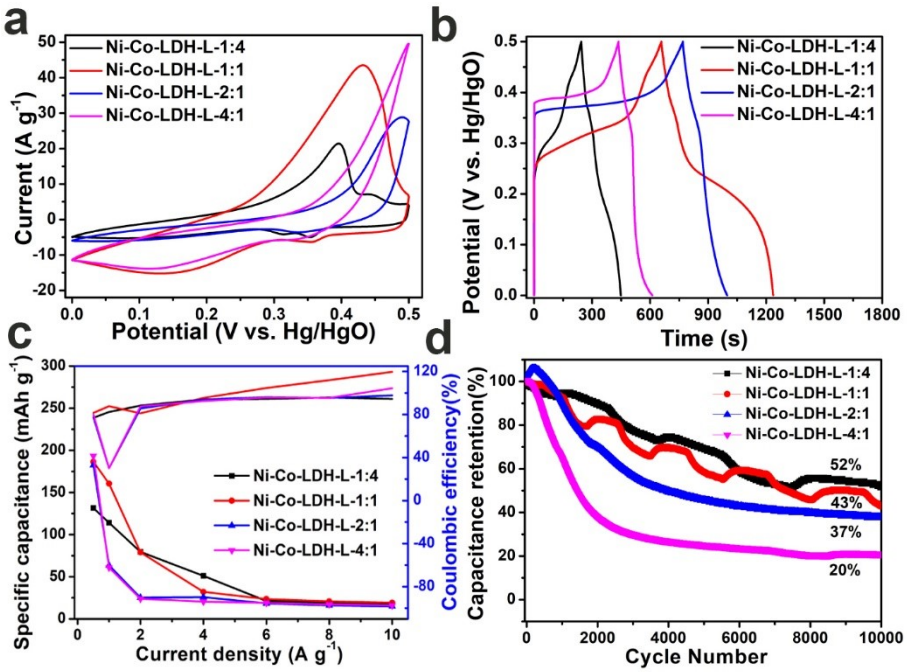

Figure S22 Electrochemical performances of Ni-Co-LDH-L-1:4, Ni-Co-LDH-L-1:1, Ni-Co-LDH-L-2:1 and Ni-Co-LDH-L-4:1 electrodes. (a) CV curves at 10 mV s^{-1}. (b) GCD curves at 1 A g^{-1}. (c) Rate capability and coulombic efficiency at different current densities. (d) Cycling performance at 6 A g^{-1}.

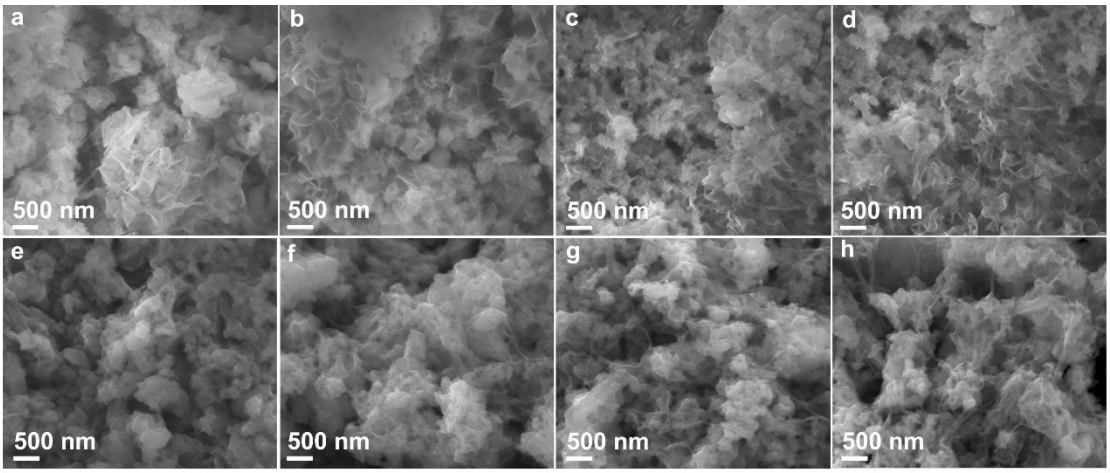

Figure S23 SEM images of Ni-Co-LDH-L-1:4, Ni-Co-LDH-L-1:1, Ni-Co-LDH-L-2:1 and Ni-Co-LDH-L-4:1 electrodes (a, b, c and d) and after the cycling test at 6 A g^{-1}(e, f, g and h).

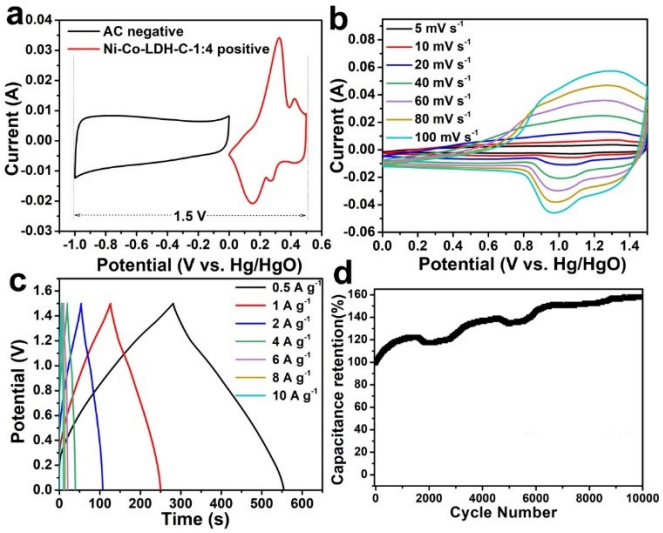

Figure. S24 (a) CV curves of the Ni-Co-LDH-C-1:4 as positive and AC negative electrodes performed in a three electrode system in 6 M KOH electrolyte at a scan rate of 10 mV s^{-1}. (b) CV curves of Ni-Co-LDH-C-1:4//AC at 0-1.5 V at various scan rates from 5 to 100 mV s^{-1}. (c) galvanostatic charge discharge curves of the device at the current densities between 0.5 and 10 A g^{-1}. (d) cycling performance with a voltage of 1.5 V at a current density of 6 A g^{-1}.

Table S4. Comparison with energy density between Ni-Co-LDH-C-1:4//AC and Ni-Co-LDH-M//AC of the present work and hybrid supercapacitors in literature.

Hybrid Supercapacitor	**Energy density @ Power density**	**Cycle life**	**Reference**
Co-Al-O_x/S_y@LSCN//LSCN	21.83 W h kg^{-1}@374.28 W kg^{-1}	4000 cycles (106%)	[11]
MCS-MXene(1:2)//AC	25.6 W h kg^{-1}@6400 W kg^{-1}	12 000 cycles (100%)	[12]
P-$NiWO_4$@$CoWO_4$//AC	26.8 W h kg^{-1}@824.6 W kg^{-1}	4000 cycles (82%)	[13]
CuO/MoS_2//BAC	26.66 W h kg^{-1}@1599.6 W kg^{-1}	5000 cycles (80%)	[14]
MIP-202 (350)//GO	16.6 W h kg^{-1}@40 kW kg^{-1}	3000 cycles (86%)	[15]
HT-Ag/ZIF(H)//AC	8.5 W h kg^{-1}@7037.04 W kg^{-1}	3000 cycles (92%)	[16]
cPNF-73//$NiCo_2O_4$	1.74 W h kg^{-1}@0.38 W kg^{-1}	2000 cycles (83%)	[17]
$CuCo_2O_4$/OMEP//AC	11.6 W h kg^{-1}@8.33 kW kg^{-1}	10 000 cycles (90%)	[18]
Ni-Co-LDH-C-1:4//AC	28.34 W h kg^{-1}@373.53 W kg^{-1}	10 000 cycles (158%)	**This work**
Ni-Co-LDH-M//AC	15.64 W h kg^{-1}@280.06 W kg^{-1}	10 000 cycles (97%)	

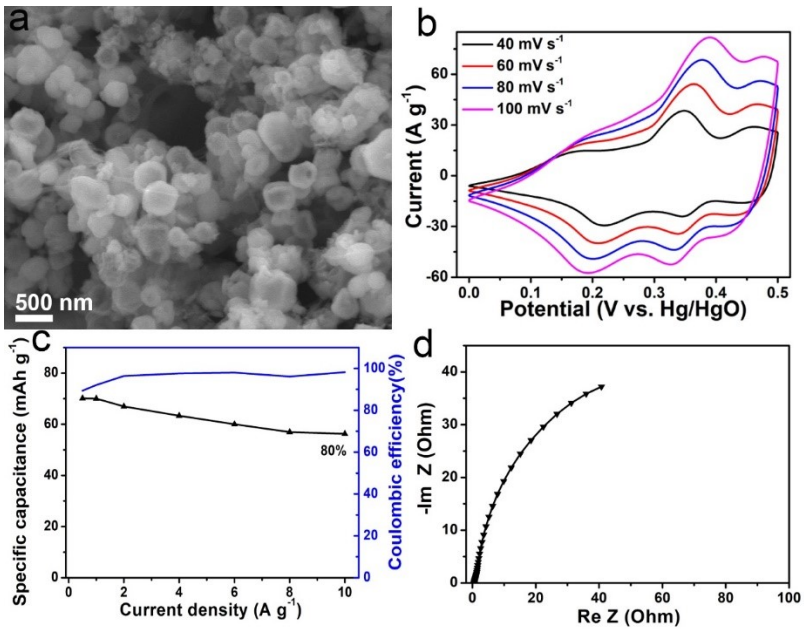

Figure S25 Electrochemical performances of Ni-Co-LDH-M electrode. (a) SEM image. (b) CV curves at different scan rates. (c) Rate capability and coulombic efficiency at different current densities. (d) Nyquist plot.

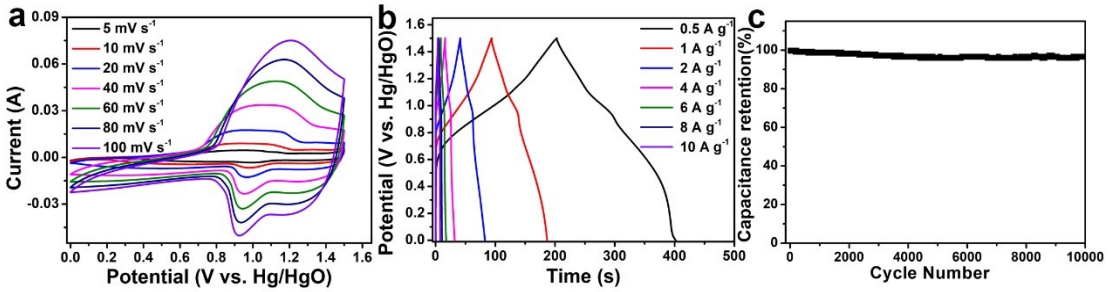

Figure. S26 (a) CV curves of Ni-Co-LDH-M//AC at 0-1.5 V at various scan rates from 5 to 100 mV s^{-1}. (b) Galvanostatic charge discharge curves of the device at the current densities between 0.5 and 10 A g^{-1}. (c) Cycling performance with a voltage of 0-1.5 V at a current density of 6 A g^{-1}.

References

[1] D. Gong, H. Tong, J. Xiao, T. Li, J. Liu, Y. Wu, X. Chen, J. Liu, X. Zhang, Self-standing manganese dioxide/graphene carbon nanotubes film electrode for symmetric supercapacitor with high energy density and superior long cycling stability, Ceramics International 47 (2021) 33020-33027.

[2] M. Sajjad, J. Ismail, A. Shah, A. Mahmood, M.Z.U. Shah, S.u. Rahman, W. Lu, Fabrication of 1.6 V hybrid supercapacitor developed using $MnSe_2$/rGO positive electrode and phosphine based covalent organic frameworks as a negative electrode enables superb stability up to 28,000 cycles, Journal of Energy Storage 44 (2021) 103318.

[3] R. Han, L. Guan, S. Zhang, Y. Lin, J. Tao, Boosted cycling stability of CoP nano-needles based hybrid supercapacitor with high energy density upon surface phosphorization, Electrochimica Acta 368 (2021) 137690.

[4] W. Wu, C. Zhao, C. Wang, T. Liu, L. Wang, J. Zhu, Hierarchical structure of Self-Supported $NiCo_2S_4$ Nanoflowers@$NiCo_2S_4$ nanosheets as high rate-capability and cycling-stability electrodes for advanced supercapacitor, Applied Surface Science 563 (2021) 150324.

[5] A.K. Das, U.N. Pan, V. Sharma, N.H. Kim, J.H. Lee, Nanostructured CeO_2/NiV-LDH composite for energy storage in asymmetric supercapacitor and as methanol oxidation electrocatalyst, Chemical Engineering Journal 417 (2021) 128019.

[6] L. Xie, S. Chen, Y. Hu, Y. Lan, X. Li, Q. Deng, J. Wang, Z. Zeng, S. Deng, Construction of phosphatized cobalt nickel-LDH nanosheet arrays as binder-free electrode for high-performance battery-like supercapacitor device, Journal of Alloys and Compounds 858 (2021) 157652.

[7] H. Liu, J. Zhu, Z. Li, Z. Shi, J. Zhu, H. Mei, Fe2O3/N doped rGO anode hybridized with NiCo LDH/$Co(OH)_2$ cathode for battery-like supercapacitor, Chemical Engineering Journal 403 (2021) 126325.

[8] F. Zhu, W. Liu, Y. Liu, W. Shi, Construction of porous interface on CNTs@NiCo-LDH core-shell nanotube arrays for supercapacitor applications, Chemical Engineering Journal 383 (2020) 123150.

[9] Y. Guo, X. Hong, Y. Wang, Q. Li, J. Meng, R. Dai, X. Liu, L. He, L. Mai, Multicomponent Hierarchical Cu-Doped NiCo-LDH/CuO Double Arrays for Ultralong-Life Hybrid Fiber Supercapacitor, Advanced Functional Materials 29 (2019).

[10] Y. Wang, F. Zheng, Q. Pan, D. Deng, L. Liu, B. Chen, A three-dimensional NiCo-LDH array modified halloysite nanotube composite for high-performance battery-type supercapacitor, Journal of Alloys and Compounds 884 (2021) 161162.

[11] C. Jiang, M. Yao, Z. Wang, J. Li, Z. Sun, L. Li, K.S. Moon, C.P. Wong, A novel flower-like architecture comprised of 3D interconnected Co-Al-Ox/Sy decorated lignosulfonate-derived carbon nanosheets for flexible supercapacitors and electrocatalytic water splitting, Carbon 184 (2021) 386-399.

[12] K. Nasrin, K. Subramani, M. Karnan, M. Sathish, $MnCo_2S_4$-MXene: A novel hybrid electrode material for high performance long-life asymmetric supercapattery, Journal of Colloid and Interface Science 600 (2021) 264-277.

[13] W. Miao, Q. Han, H. Zhang, K. Chen, L. Zhang, Y. Li, S. Han, Uniform phosphorus doped CoWO4@$NiWO_4$ nanocomposites for asymmetric supercapacitors, Journal of Alloys and Compounds 877 (2021) 160301.

[14] G.P. Awasthi, M.B. Poudel, M. Shin, K.P. Sharma, H.J. Kim, C. Yu, Facile synthesis of a copper oxide/molybdenum disulfide heterostructure for asymmetric supercapacitors of high specific energy,

Journal of Energy Storage 42 (2021) 103140.
[15] M. Rad, S. Borhani, M. Moradi, V. Safarifard, Tuning the crystallinity of ZrO_2 nanostructures derived from thermolysis of Zr-based aspartic acid/succinic acid MOFs for energy storage application, Physica E: Low-dimensional Systems and Nanostructures 134 (2021) 114921.
[16] M. Pooriraj, M. Moradi, S. Hajati, Impact of silver incorporation on cobalt rich 3-D porous carbon arising from solid state thermolysis of ZIF-67 as a pseudocapacitor electrode: Improvement of diffusion-controlled charge storage, Solid State Ionics 368 (2021) 115697.
[17] M.J. Ma, J.G. Seong, S. Radhakrishnan, T.H. Ko, B.S. Kim, Preparation of Network-Structured Carbon Nanofiber Mats Based on PAN Blends Using Electrospinning and Hot-Pressing Methods for Supercapacitor Applications, Nanomaterials (Basel) 11 (2021).
[18] M. Li, Z. Meng, R. Feng, K. Zhu, F. Zhao, C. Wang, J. Wang, L. Wang, P.K. Chu, Fabrication of Bimetallic Oxides (MCo_2O_4: M=Cu, Mn) on Ordered Microchannel Electro-Conductive Plate for High-Performance Hybrid Supercapacitors, Sustainability 13 (2021).